



Contents lists available at ScienceDirect

Journal of King Saud University – Science

journal homepage: www.sciencedirect.com

Original article

Cytotoxic and molecular assessment with copper and iron nanocomposite, act as a soft eradicator against cancer cells

Rizwan Wahab^{a,b,*}, Farheen Khan^{c,*}, Javed Ahmad^a, Abdulaziz A. Al-Khedhairy^{a,b}^a Chair for DNA Research, College of Science, Department of Zoology, King Saud University, Riyadh 11451, Saudi Arabia^b Zoology Department, College of Science, King Saud University, P.O. Box 2455, Riyadh 11451, Saudi Arabia^c Chemistry Department, Faculty of Science, Taibah University, Madina (Yanbu), Saudi Arabia

ARTICLE INFO

Article history:

Received 19 December 2021

Revised 13 January 2022

Accepted 9 February 2022

Available online 15 February 2022

Keywords:

Nanocomposite

SEM

TEM

MTT assay

qPCR

ABSTRACT

The composites are the materials, which have either one or more combination with other material and exhibit extraordinary chemical characteristics. The present work describes the formation of composite of copper and iron metal oxide (CuFeO₂). The synthesized powder materials are in nanorange. The nanocomposite nanoparticles (NCsNPs) were synthesized via solution process with using copper nitrate hexahydrate, iron nitrate non hydrate as a main precursor material whereas sodium hydroxide was utilized as a salt reducing agent. The formed NCsNPs were characterized with X-ray diffraction pattern (XRD), Scanning electron microscopy (SEM), Transmission electron microscopy (TEM) and Fourier Transform infra-red spectroscopy (FTIR) were used for the structural and chemical characteristic in detail. It reveals that the NCNP is ~45 nm in size with clear spherical shaped morphology with good chemical characteristics. The NCsNPs were utilized against cancer cells (C2C12 myoblast) for to reduce the growth rate with different incubation (24 & 48 h) periods. The % cells death was examined through MTT assay at different concentration (0.5 µg/mL, 1 µg/mL, 2 µg/mL, 5 µg/mL, 10 µg/mL, 25 µg/mL, 50 µg/mL, 100 µg/mL) of NCs with different (24 & 48 h) incubations respectively. The apoptosis in cells were analyzed with quantitative polymerase chain reaction (qPCR) study with apoptotic marker gens caspase 3 and 7 with control and the obtained data reveals that with the exposure of NCs, upregulated in gene expression at fixed concentration in 24 h incubation period. Based on acquired results a possible relation between the NCs and cancer cells were also discussed.

© 2022 The Author(s). Published by Elsevier B.V. on behalf of King Saud University. This is an open access article under the CC BY-NC-ND license (<http://creativecommons.org/licenses/by-nc-nd/4.0/>).

1. Introduction

The nanoscience and nanotechnology provide a range of different shapes and size of nanostructures, which have technological aspect and applied in various fields (Bayda et al., 2020). The structures are zero, one or two dimensional shapes and these structures can be possible to process with physical and chemical methods for

the applications in various directions (Velický and Toth, 2017). Amid various single metal oxide nanostructures (such as zinc oxide, copper oxide, nickel oxide, magnesium oxide, iron oxide, tin oxide etc.) (Chavali and Nikolova, 2019), the mixed metal oxides/composites exhibit the possibility to generate a new inter-dependent properties and it improves the overall application performance due to wide band gap and appropriate combination of individual oxide components (Hong et al., 2020). The composites are the materials, which have two or more different constituent materials, and each exhibit their own significant characteristic and combined together to create a new material/substance with superior properties than the original materials in a specific finished structure. The nanocomposites (NCs) are those materials, which have the nanostructural morphology such as nanoparticles, tubes, rods etc. They are in multi-phasic property with dimensions ranges from 10 to 100 nm. NCs are the best alternative for the single oxide nanostructured material because it exhibit the larger band gap and enhanced volume ratios. It can be classified based on their matrix in dispersed phases (Sen, 2020; Ngo, 2020). NCs have improved

* Corresponding authors at: Chair for DNA Research, College of Science, Department of Zoology, King Saud University, Riyadh 11451, Saudi Arabia (R. Wahab) and Chemistry Department, Faculty of Science, Taibah University, Madina (Yanbu), Saudi Arabia (F.Khan).

E-mail addresses: rwahab@ksu.edu.sa (R. Wahab), fsharef@taibahu.edu.sa (F. Khan).

Peer review under responsibility of King Saud University.



Production and hosting by Elsevier

physical and chemical properties as compared to single oxides such as high thermal stability, improved surfaces, superior electrical conductivity, enhanced chemical resistance and high optical property etc (Camargo et al., 2009, Khan et al., 2019; Jeevanandam et al., 2018). The NCs offers unique properties, which arises from their small size, enhanced surface area, high interfacial interaction between the phases (Torrise and Ruffino, 2015). Their unique property facilitates to utilize for to enhance the biological activity of many drugs, biomaterials, catalysts, and also in some high-value added materials (Li et al., 2020). The NCs can be classified by two major categories such as polymeric (polymer organic, inorganic and hybrid) and non-polymeric (metal, ceramic and ceramic-ceramic NCs) (Sen, 2020; Jeon and Baek, 2010; Khorshid et al., 2020). A number of ways were applied for the preparation of NCs with physical and chemical procedure's for instance plasma and hot chemical vapor deposition (Bita et al., 2020, Wu et al., 2019), co-precipitations (Nithiyantham et al., 2021), sol-gel (Sheng et al., 2019), solvothermal (Zhan et al., 2019), micro-emulsion (Li et al., 2019), combustion (Trusiano et al., 2019), vapor condensation (Patelli et al., 2019), spray pyrolysis (Leng et al., 2019), template and surface derivatized methods and various others (Fan et al., 2019). The cost is a crucial factor for the preparation of such NCs and impacted a critical influence on the structural morphology, subsequently effect on technological applications. Within various types of synthesis procedures, the chemical solution/co-precipitation is the best way to form versatile morphology of the nanostructures (Chen et al., 2019). The NCs exhibit the capability to optimize the size of nanostructures, applied in various directions such as it hold drugs and deliver to the target entities, functionalize the surfaces, chemical and biological sensors also released the drug in blood for longer period, also exhibit great impact and high potential to deal numerous characteristics (Wahab et al., 2020a). Among various biological applications in different discipline very limited studies are available for the application of NCs are available.

A number of research had been done related to the application of NPs and related nanostructures in the area of biomedical applications (Ojo et al., 2021) but very limited studies are available related to use of NCs in cancer studies. To keep this view the present work was design and implemented for C2C12 cancer cell lines. For this, copper and iron oxide (CuFeO₂) NCs nanoparticles (mentioned to as CuFeO₂NCsNPs) processed via chemical process and were well analyzed. Beside these, the control (without CuFeO₂NCsNPs) and treated cancer cells morphology with CuFeO₂NCsNPs were examined via inverted microscopy. The viable and non-viable cells of toxicities were studied via MTT assays. Beside these gene expressions were also conducted with caspase 3/7 with control (GAPDH) gene in cancer cells after the exposure of 24 h of incubation. Based on the obtained results a discussion was also proposed.

2. Material and methods

2.1. Experimental

2.1.1. Synthesis of copper based iron oxide nanocomposite (CuFeO₂NCs)

For the formation of NCs, the chemicals such as copper nitrate hexahydrate (Cu(NO₃)₂·6H₂O), iron nitrate non hydrate (Fe(NO₃)₂·9H₂O), sodium hydroxide (NaOH) were procured from Sigma-Aldrich chemical corporation and used without any further modification. To perform successful synthesis, copper nitrate hexahydrate (Cu(NO₃)₂·6H₂O, 3 × 10⁻²M), iron nitrate nonhydrate (Fe(NO₃)₂·9H₂O, 3 × 10⁻²M) were mixed in 100 mL of methanol (MeOH) solvent. Once the solution was completely dissolved, alkaline solution of NaOH (0.1 M) was added to this mixture for to form

the hydroxide molecules of double salt under constant stirring for ~20 min. The solution pH (cole-parmer, U.S.A) was measured and reached up to 12.70. The obtained solution was transferred it to a refluxing flask and refluxed at 80 °C for ~60 min under continuous stirring condition, and observed in the refluxing pot, once the heating temperature surges, the color of solution turns from dark red to black. Once the set reaction was completed, the precipitated product was cooled at room temperature, washed well with alcohol and dried the product at room temperature and to store for further analysis.

2.2. Characterizations of the prepared powder material (CuFeO₂NCs)

The crystalline character, phases, size of the prepared powder were examined via X-ray diffraction pattern (XRD, PANalytical XPert Pro, Colorado, U.S.A.) with CuK_α radiation ($\lambda = 1.54178 \text{ \AA}$) in range from 20 to 80° with 6°/min scanning speed. The morphological observation was confirmed via SEM (JEOL, JED-2200 series, Tokyo, Japan) at room temperature. To analyse the processed powder morphology, sprinkled homogeneously on a carbon tape and pasted on sample holder. The sample holder was moved to sputtering chamber, where conducting layer of platinum (Pt) was coated for ~3 s. The sample was fixed in a sample holder and analyzed the morphology at room temperature. Further the morphological investigation was again analyzed via TEM (JEOL, JSM, 2010, Tokyo, Japan). The functional chemical bonding in terms of asymmetric and symmetric stretching mode of vibrations between the metal and oxygen were confirmed via Fourier transform infrared (FTIR; Perkin Elmer-FTIR Spectrum-100, Shelton, C.T, U.S.A.) spectroscopy analyzed within the range of 4000–400 cm⁻¹.

2.3. Cells culture

The cells (C2C12) were purchased from American Type Culture and collection (ATCC, U.S.A). The procured cells vial were thawed at 37 °C for 2–3 min and then after transferred it to a 75 mm² flask and cultured with cell culture medium (Dulbecco's Modified Eagle's Medium, DMEM) containing 10–12% fetal bovine serum (FBS), 100 IU/mL penicillin, and 100 µg/mL streptomycin) in a humid environment incubated at 37 °C with 5% CO₂. The medium was refilled at an alternate day and were subcultured after reached 85–90% confluence.

2.4. MTT assay

The % cells viability was examined via using cell proliferation kit I (MTT, ROCHE, Ltd, U.S.A) and utilized as per instructions. The cells were initially cultured in a 96-wells plates with concentration range ~1 × 10⁴ and nurtured the plate for 24 h at 37 °C in an incubator with 5% CO₂. When the cells were reached to their optimal confluence, the different concentrations of NCs (0.5 µg/mL, 1 µg/mL, 2 µg/mL, 5 µg/mL, 10 µg/mL, 25 µg/mL, 50 µg/mL, 100 µg/mL) were mixed it and to keep the solution in an incubator for 24 and 48 h. For the viability test of the cells with NCs, the MTT assay ((3-(4,5-dimethyl thiazol-2-yl)-2,5-diphenyltetrazolium bromide, 10 µL/well)) was mixed with cell culture solution. Including the control solution, the MTT solution was added with NCs samples and again incubated the culture solution at 37 °C for 4 h. When the incubation period was accomplished the sample was moved from the incubator and to this sample a solubilizing buffer (100 µL/well) was mixed. In the culture flask, a purple color solution was appeared and it fainted over pipetting. Due to MTT assay as formazan precipitate was formed and it dissolved with DMSO in both control and treated samples. The % viability was tested with MTT assay through Elisa Reader (Bio Rad, 570 nm). The absorbance of purple color solution was measured through spectrophotometer

at usually ~ 570 nm wave length. The percentage (%) viability was calculated as follows:

$$\% \text{ Viability} = \text{OD (optical densities) in sample well} / \text{OD in control well} \times 100$$

2.5. qPCR study

The RNA was extracted from the cultured cells with at low and high concentration of the treated material with selective protocol via Trizol as per according to the manufacturer's protocol. The purity of RNA was examined via the optical density between 260 and 280 nm. The cDNA was formed with using M-MLV reverse transcriptase as acknowledged in the literature (Wahab et al., 2016). The intensities of genes bands were measured from quantity one program (Bio-Rad, USA) through gels electrophoresis.

2.6. Statistical analysis

The statistical assessments were expressed and authenticated the student T-test, mean \pm SD and standard pool at significant value ($P < 0.05$).

3. Result and discussions

3.1. X-ray diffraction (XRD) results

XRD provide the information related to the processed powder crystallite size, phases and crystalline of the material. In this experiment, the analysis was performed in range of $20\text{--}80^\circ$ with $6^\circ/\text{min}$ scanning speed with 40 kV and 30 mA current. The obtained spectroscopic data reveals that all peaks and their corresponding positions are very clear such as $\langle 006 \rangle$ (30.13), $\langle 012 \rangle$ (35.33), $\langle 015 \rangle$ (43.21), $\langle 018 \rangle$ (57.18) and $\langle 110 \rangle$ (62.73) are with powder diffraction data analogous with Joint Committee on Powder Diffraction Standards (JCPDS) with card number 039-0246. The acquired crystal geometry of rhombohedral space group R_3m with lattice constant were $a_h = 53.03 \text{ \AA}$ and $c_h = 517.09 \text{ \AA}$ respectively (Fig. 1) (Galakhov et al., 1997). In all the defined peaks show that the material is highly crystalline with defined facts. The diffraction pattern also shows that there is no other peaks related to impurity was formed except the processed material NCs, which again validates that the material is pure oxide nanomaterials. Average crystallite size and other parameters such as phases, peaks

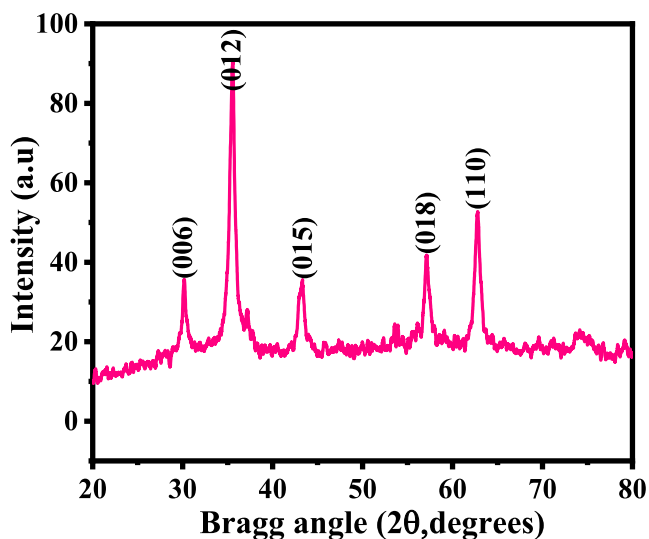


Fig. 1. XRD pattern of NCs via solution process.

positions, FWHM of the processed powder was calculated to $\sim 44 \pm 1$ nm through well-known Scherer equation (Cullity, 1978).

3.2. Morphological evaluation of the processed powder

The powder morphology was examined through SEM and obtained data is presented as Fig. 2. The low (Fig. 2a) and high (Fig. 2b) magnification scales shows that in a larger amount of NCsNPs are seen in a wide captured areas. Several particles are seen in the images, some are combined with other one and some are seems to be separate and single. The powder was also checked at high magnification scale and found that the entire surface was full of spherical shaped nanostructures, with combined to other nanospheres (Fig. 2c & d). The grown crystallite surfaces exhibit a defined shape with full array bunches of nanostructures with an organized in manner.

Further for more detailed observation related to the structural assessment of the prepared powder, sample was again checked via TEM and the obtained result is presented as Fig. 3. From the obtained images it illustrates that NCs are in a grouped with other particles (Fig. 3) with spherical in shape. The average diameter of each nanoparticle is in the range of 45–50 nm in size (Fig. 3). The data's are in full consistent with SEM and XRD observations (Figs. 1 & 2).

3.3. FTIR spectroscopy results of NCs

Fig. 4. Shows the FITR results of the prepared powder, which shows a wide and shallow band observed in the range of $3200\text{--}3600 \text{ cm}^{-1}$ designates the hydroxyl (H–O–H, 3340 cm^{-1}) group vibration mode (Barnabé et al., 2013). The small peak at 2341 cm^{-1} designates the atmospheric CO_2 whereas the sharp peak observed at 1641 cm^{-1} shows the vibrational mode of hydroxyl group (–OH) molecule. The vibrations of nitro group (NO_3^-), was observed at 1053 cm^{-1} respectively. The oxide peaks was observed at 602 cm^{-1} and it demonstrates the formation of nanocomposite (CuFeO_2). From the obtained data and their peaks observations reveals that the –OH group changes to the oxides and shows the formation of NCs (Fig. 4) (Schmachtenberg et al., 2019).

3.4. Morphology of cultured cells visualized via microscopy

The cells were cultured in a culture medium DMEM and incubated at defined time intervals 24 (Panel A) and 48 h (Panel B). When the cells were incubated and reached to their optimal confluence, the cells morphologies were captured as treated (with NCs) and control (without NCs) cells and presented as Fig. 5. The cells were exposed with different concentration of NCs (0.5 $\mu\text{g}/\text{mL}$, 1 $\mu\text{g}/\text{mL}$, 2 $\mu\text{g}/\text{mL}$, 5 $\mu\text{g}/\text{mL}$, 10 $\mu\text{g}/\text{mL}$, 25 $\mu\text{g}/\text{mL}$, 50 $\mu\text{g}/\text{mL}$, and 100 $\mu\text{g}/\text{mL}$) at different incubations (24 and 48 h) period. Initially, single cells were seen at many places were as it's nucleated upon their confluence. The nucleated/confluence cells were exposed with NCs at an above mentioned condition. From the recovered images, it's very clear that as the doses of NCs increases with the cells, the cancer cells growth were much affected and high density of cells were reduced (Fig. 5) (Wahab et al., 2016).

3.5. MTT assay results with nanostructures

From the MTT assay cells proliferation rate was to measure under the manner of treated and untreated (control). The data received from the MTT assay shows that the cell death or inhibitory effects dependent on dose dependent manner against cancer cells. The cultured cells were incubated with NCs with different concentrations (0.5 $\mu\text{g}/\text{mL}$, 1 $\mu\text{g}/\text{mL}$, 2 $\mu\text{g}/\text{mL}$, 5 $\mu\text{g}/\text{mL}$, 10 $\mu\text{g}/\text{mL}$,

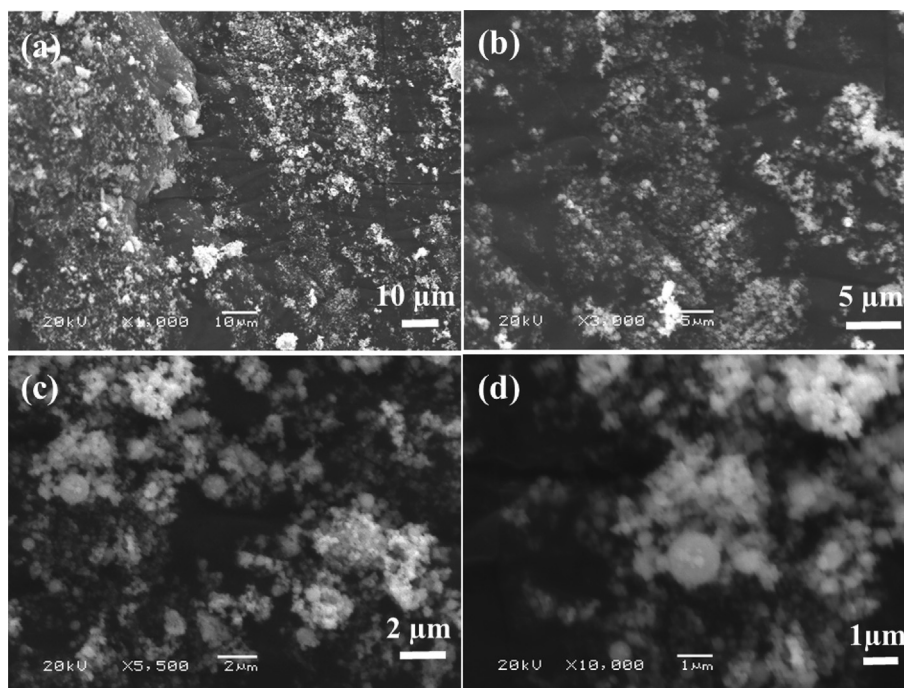


Fig. 2. SEM images of NCs: at low magnification (a) and (b) high magnification.

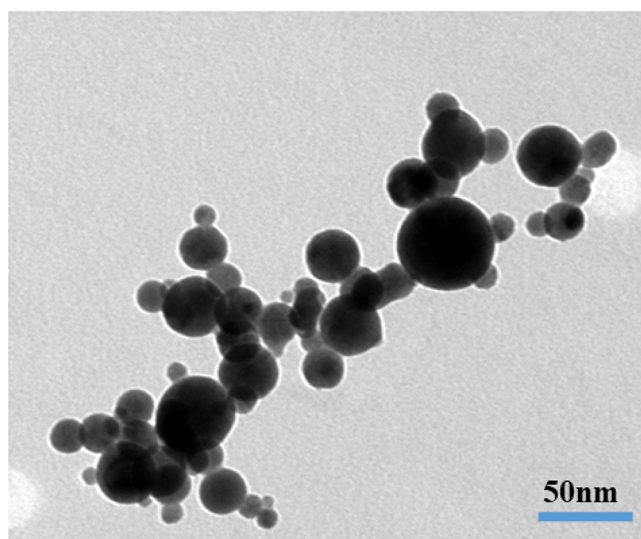


Fig. 3. Displayed the low magnification TEM images of NCs.

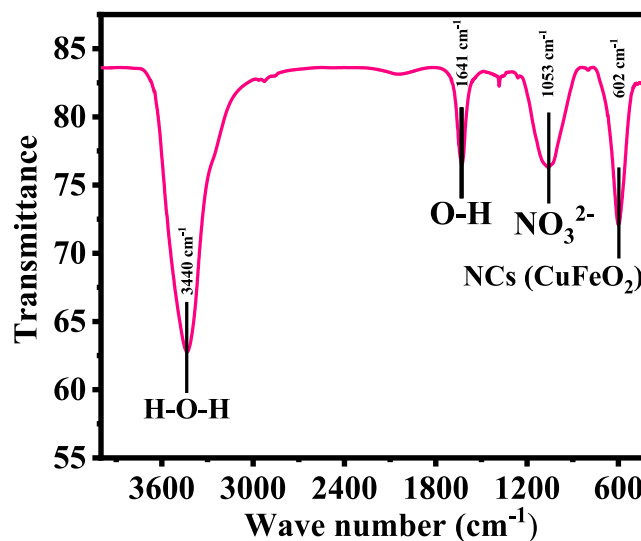


Fig. 4. Shows the FTIR spectra of grown NCs.

25 $\mu\text{g/mL}$, 50 $\mu\text{g/mL}$, 100 $\mu\text{g/mL}$). With this, a series of different concentration also included control to compare the growth rate of cancer cells continuously. The cells were washed to remove the medium and % cell death was determined through MTT method (Wahab et al., 2016). A significant change was observed at low concentration of the material but as the doses were increased the cells viability was much influenced. The cells viability at different concentrations at 0.5 $\mu\text{g/mL}$, 1 $\mu\text{g/mL}$, 2 $\mu\text{g/mL}$, 5 $\mu\text{g/mL}$, 10 $\mu\text{g/mL}$, 25 $\mu\text{g/mL}$, 50 $\mu\text{g/mL}$, 100 $\mu\text{g/mL}$ of, NCs are 101%, 100%, 93%, 88%, 78%, 64%, 51% and 35% of the cells, respectively. The cells demise were varied at 48 h for the concentrations of 0.5 $\mu\text{g/mL}$, 1 $\mu\text{g/mL}$, 2 $\mu\text{g/mL}$, 5 $\mu\text{g/mL}$, 10 $\mu\text{g/mL}$, 25 $\mu\text{g/mL}$, 50 $\mu\text{g/mL}$, 100 $\mu\text{g/mL}$ of, NCs are 90%, 89%, 84%, 75%, 66%, 49% and 37%, 21% of the cells, respectively (Fig. 6). The interaction of NCs with cancer cells and their % reduction express that NCs

are much effective and can be possible to utilize as anticancer agents (Wahab et al., 2018).

3.6. qPCR study induced by NCs

RNA expression was also analyzed with qPCR with NCs in presence of caspase gens (3/7) with cancer cells at low and high concentration of the material and NCs (25 $\mu\text{g/mL}$) and high (50 $\mu\text{g/mL}$) at 24 and 48 h incubation time respectively. The obtained data reveals that in 24 and 48 h of incubation caspase 3 with NCs were express 2.52 and 3.75 fold changes respectively at low concentration of NCs (25 $\mu\text{g/mL}$). The data reveals that both the genes were up-regulated. At higher concentration of NCs (50 $\mu\text{g/mL}$), a sequential changed has been observed and it was examined from 3.64 to 5.85 fold change in 24 & 48 h incubation period respectively. The

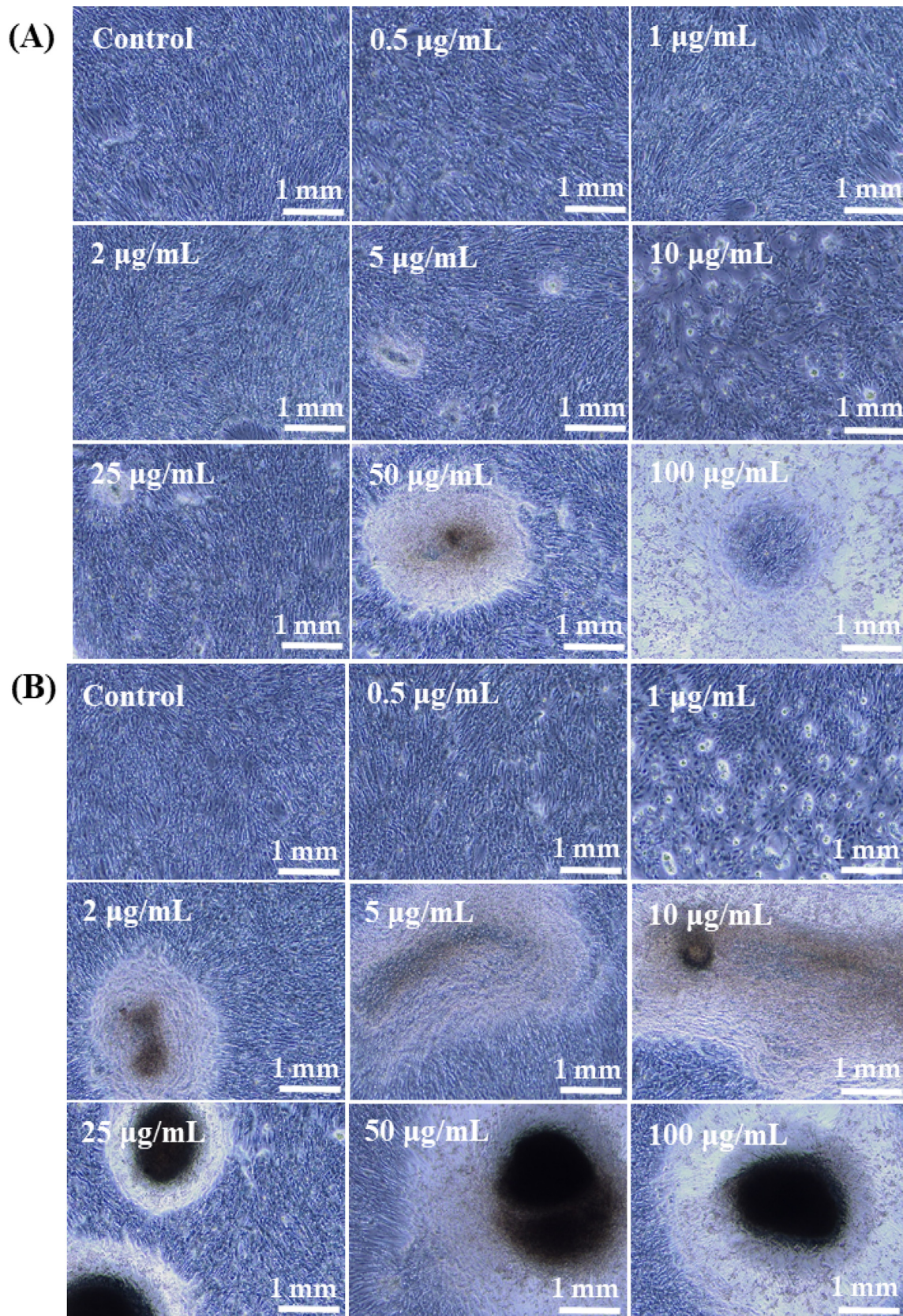


Fig. 5. The microscopic images of cultured cells and their interaction with NCs at different concentrations, where Panel A at 24 h and Panel B at 48 h incubations respectively.

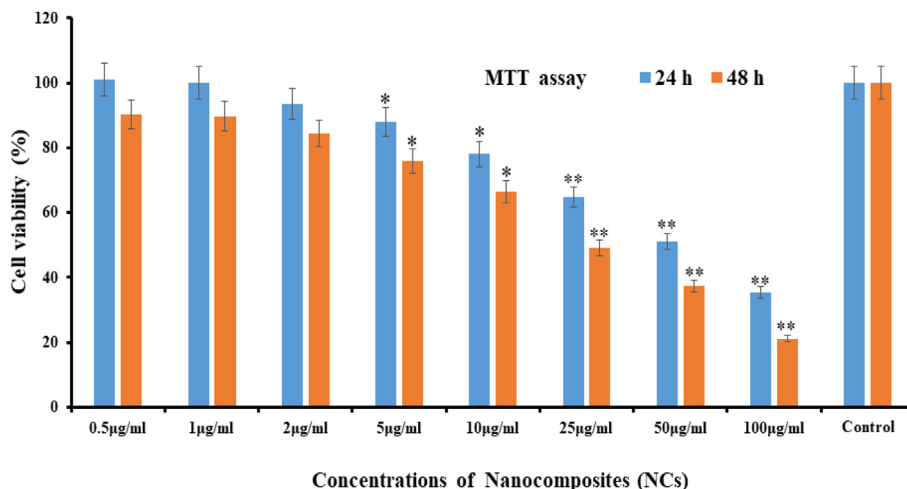


Fig. 6. MTT assay at different time (24 & 48 h) intervals with control solution. *p < 0.01, **p < 0.001 Vs Control. The data represent as of three identical experiments.

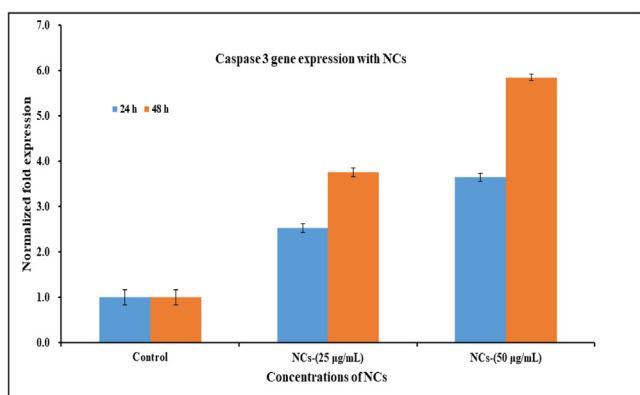


Fig. 7. Effect of NCs on mRNA expression level of C2C12 cells for caspase 3 at alternate incubation periods (24 & 48 h) in presence of control gene (GAPDH) for the normalization of data reacted with NCs at low (25 µg/mL) and high (50 µg/mL) concentration. The data represent as mean ± SD of three identical experiments with three replicates.

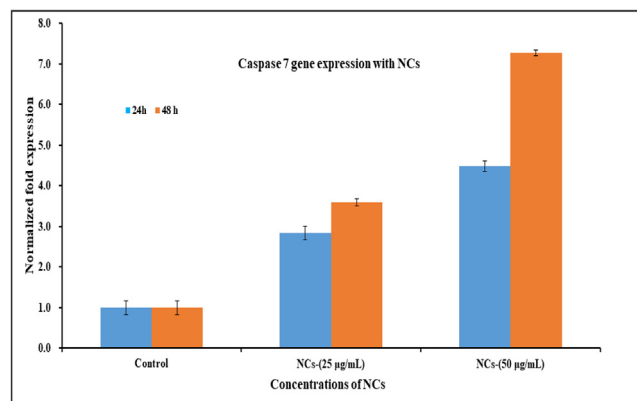


Fig. 8. Effect of NCs on mRNA expression level mRNA expression level of C2C12 cells for caspase 7 at an alternate incubation periods (24 & 48 h) in presence of control gene (GAPDH) for the normalization of data reacted with NCs at low (25 µg/mL) and high (50 µg/mL) concentration. The data represent as mean ± SD of three identical experiments with three replicates.

recovered data displayed that the employed NCs in causes the up-regulation expression and indicates the apoptosis in cells with caspase 3 genes (Fig. 7). The previous studies (Wahab et al., 2016; 2018) discloses that activities of caspases are responsible and narates to affect the apoptotic cells, which are present in naturally growing cells. It also examined that the enhance fold change in caspases are liable in cancer cells, when treated with NCs and compared with the control gene (GAPDH). As per previous published literature (Wahab et al., 2016; 2018), that oxide based nanostructures play a deadly substance for the growth of cancer cells. The cells apoptosis are influenced directly or indirectly with various parameters such as higher doses of used nanostructured materials, culture medium concentrations, high rate of incubation and others, increases the apoptosis in cells and resulted an up-regulation in mRNA expression. The similar results were also found with caspase 7, once reacted with NCs at 24 & 48 h incubations. The cells were incubated at 24 h and at low concentration of NCs (25 µg/mL), the caspase 7 expressed 2.83 fold changes whereas at higher doses of NCs (50 µg/mL), the rate of apoptosis increased 4.48 fold change (Fig. 8) (Wahab et al., 2016; 2018). At low concentration of NCs (25 µg/mL), caspase 7 expressed to 3.59 whereas at higher concentration of NCs (50 µg/mL) its increased 7.28 fold change with 48 h incubation period.

3.7. Discussions

On the basis of obtained results and their observations, a possible discussion related to cytotoxicity of cancer cells with NCs discussed. As according to the previously published research work (Wahab et al., 2014), the toxicity in cancer cells were much influenced with the inorganic based oxide nanostructures and other numerous physicochemical parameters for instance crystallite size, morphology of nano structures, utilized chemicals, different materials, concentration of nanostructures, incubation period of cells, cultured cells concentration, endocytic uptake of cells etc (Wahab et al., 2014). In the present case, the prepared NCs utilized and at initially the NCs were interacted on the upper layer of cancer cells. Due to very small size of the NCs and each cell, which have very small pores to provide easy passage for the entrance of NCs on the upper surface of cancer cells and due to very small size of each NC is ~45 nm as compared to the individual cell size (~18–20 µm), it can be enter easily in cells. In a culture medium the enhanced density of NCs sturdily favors formation of aggregated molecules (Wahab et al., 2014, 2012, 2020b) and postulates that these NCs destroy the internal cells organelles and are liable for cells death. The current approach is also justified with the available results such as microscopy, MTT and it reveals the cells death as

with dose dependent manner (Wahab et al., 2021a,b). MTT assay provides the quantitative analysis of the control and treated cells and it shows that the initial concentration of applied NCs are not much affected on the growth of cancer cells were as once the concentrations of NCs roses, the cells growth were much influenced (Wahab et al., 2021a). The apoptosis in cells leads the cells death caused with the NCs and it analyzed via gene expression study, also justified and in consistent. Several other biochemical studies are required to disclose the phenomena why these structures (NCs) are responsible to control/regulate the growth or cell death of cancer cells (Wahab et al., 2021a). Why the NCs are responsible for the retardation of cancer cells growth and biochemical mechanism is under way to find out the exact research detail.

4. Conclusions

The summary of the present work describes that the nanocomposite (CuFeO₂NCsNPs) were formed via solution process and the obtained product was characterized well. The XRD pattern reveals that the processed material exhibit good crystallinity with an average size ~45 nm, whereas SEM indicates that each particle are smooth with clear surfaces and rounded in shape. The morphological clarification was further confirmed via TEM which states that the particle size is ~45 nm and it analogous with SEM observations. The FTIR spectroscopy confirms the formation of composite of copper and iron oxide (CuFeO₂). The NCs were utilized against to retard the growth of cancer cells. The % cells death were examined from the MTT assay and it reveals that at low doses of NCs shows less cells death, whereas once the doses were increased the % cells death were enhanced more and more. The cells deaths were also affected with incubation period which is an important factor for the cells reduction, and it seems less but when the dose of NCs were increases it effectively reduces the cells growth. The cells apoptosis with NCs were also studied in presence of caspase 3/7 and it illustrates that the NCs are responsible for the apoptosis in cancer cells. Based on the acquired data and their observations a mechanism related to the interaction of NCs and cancer cells are also explained. The current study provides the new insights to control and regulate the cancer cells with using a low cost nanostructured material, because a number of therapies (chemotherapy, radiotherapy, immunotherapy etc) and surgery are utilized, which are very costly and difficult to afford for the deprived and low income families.

Declaration of Competing Interest

The authors declare that they have no known competing financial interests or personal relationships that could have appeared to influence the work reported in this paper.

Acknowledgement

The authors are grateful to the Deanship of Scientific Research, King Saud University for funding through Vice Deanship of Scientific Research Chairs.

References

Bayda, S., Adeel, M., Tuccinardi, T., Cordani, M., Rizzolio, F., 2020. The history of nano science and nanotechnology: from chemical-physical applications to nano medicine. *Molecules* 25 (1), 112.
Bita, B., Vizireanu, S., Stoica, D., Ion, V., Yehia, S., Radu, A., Iftimie, S., Dinescu, G., 2020. On the structural, morphological, and electrical properties of carbon nano walls obtained by plasma-enhanced chemical vapor deposition. *J. Nano Mater.* 2020, 1–6.

Barnabé, A., Chapelle, A., Presmanes, L., Tailhades, P., 2013. Copper and iron based thin film nanocomposites prepared by radio frequency sputtering. Part I: elaboration and characterization of metal/oxide thin film nanocomposites using controlled in situ reduction process. *J. Mater. Sci.* 48 (9), 3386–3394.
Chavali, M.S., Nikolova, M.P., 2019. Metal oxide nanoparticles and their applications in nanotechnology. *SN Appl. Sci.* 1, 607.
Chen, G., Zhang, X., Gao, Y., Zhu, G., Cheng, Q., Cheng, X., 2019. Novel magnetic MnO₂/MnFe₂O₄ nanocomposite as a heterogeneous catalyst for activation of peroxy-monosulfate (PMS) toward oxidation of organic pollutants. *Sep. Purif. Technol.* 213, 456–464.
Camargo, P.H.C., Satyanarayana, K.G., Wypych, F., 2009. Nanocomposites: synthesis, structure, properties and new application opportunities. *Mater. Res* 12 (1), 1–39.
Cullity, B.D., 1978. *Elements of X-ray Diffraction*. Addison-Wesley Publishing Company, Reading, MA.
Fan, D., Wang, G., Ma, A., Wang, W., Chen, H., Bai, L., Yang, H., Wei, D., Yang, L., 2019. Surface engineering of porous carbon for self-healing nanocomposite hydrogels by mussel-inspired chemistry and PET-ATRP. *ACS Appl. Mater. Interfaces* 11 (41), 38126–38135.
Galakhov, V.R., Poteryaev, A.I., Kurmaev, E.Z., Anisimov, V.I., 1997. Valence-band spectra and electronic structure of CuFeO₂. *Phys. Rev. B* 56 (8), 4584–4591.
Hong, X., Wang, X., Li, Y., Fu, J., Liang, B., 2020. Progress in graphene/metal oxide composite photocatalysts for degradation of organic pollutants. *Catalysts* 10 (8), 921.
Jeon, I.Y., Baek, J.B., 2010. Nanocomposites derived from polymers and inorganic nano particles. *Materials (Basel)* 3 (6), 3654–3674.
Jeevanandam, J., Barhoum, A., Chan, Y.S., Dufresne, A., Danquah, M.K., 2018. Review on nanoparticles and nanostructured materials: history, sources, toxicity and regulations. *Beilstein J. Nanotechnol.* 9, 1050–1074.
Khan, I., Saeed, K., Khan, I., 2019. Nanoparticles: properties, applications and toxicities. *Arabian J. Chem* 12 (7), 908–931.
Khorshid, M.T., Kumar, A., Omrani, E., Kim, C., Rohatgi, P., 2020. Synthesis, characterization, and properties of graphene reinforced metal-matrix nanocomposites. *Composites Part B: Eng.* 183, 107664.
Li, X., Liu, L., Xu, Z., Wang, W., Shi, J., Liu, L., Jing, M., Li, F., Zhang, X., 2019. Gamma irradiation and microemulsion assisted synthesis of monodisperse flower-like platinum-gold nanoparticles/reduced graphene oxide nanocomposites for ultra sensitive detection of carcinoembryonic antigen. *Sens. Actuators B: Chem.* 287, 267–277.
Li, B., Elango, J., Wu, W., 2020. Recent advancement of molecular structure and bio material function of chitosan from marine organisms for pharmaceutical and nutraceutical application. *Appl. Sci.* 10 (14), 4719.
Leng, J., Wang, Z., Wang, J., Wu, H.-H., Yan, G., Li, X., Guo, H., Liu, Y., Zhang, Q., Guo, Z., 2019. Advances in nanostructures fabricated via spray pyrolysis and their applications in energy storage and conversion. *Chem. Soc. Rev.* 48 (11), 3015–3072.
Ngo T.D., 2020. *Introduction to Composite Materials, Composite and Nano composite Materials*, Intech open book Series, ISBN: ISBN: 978-1-78985-461-9.
Nithiyantham, S., Viviliya, S., Anandhan, S., Mahalakshmi, S., 2021. Synthesis and characterization of cobalt ferrite through co-precipitation technique. *Lett. Appl. Nano BioSci* 10 (1), 1871–1876.
Ojo, O.A., Olayide, I.I., Akalabu, M.C., Ajiboye, B.O., Ojo, A.B., Oyinloye, B.E., Ramalingam, M., 2021. Nanoparticles and their biomedical applications. *Biointerface Res. Appl. Chem.* 11 (1), 8431–8445.
Patelli, N., Migliori, A., Morandi, V., Pasquini, L., 2019. One-step synthesis of metal/oxide nanocomposites by gas phase condensation. *Nanomaterials* 9 (2), 219.
Sen M., 2020. *Nanocomposite Materials, Nanotechnology and the Environment*, Intech open book Series, ISBN: 978-1-78985-671-2.
Sheng, Y., Yang, J., Wang, F., Liu, L., Liu, H., Yan, C., Guo, Z., 2019. Sol-gel synthesized hexagonal boron nitride/titania nanocomposites with enhanced photocatalytic activity. *Appl. Surf. Sci.* 465, 154–163.
Schmachtenberg, N., Silvestri, S., da Silveira Salla, J., Dotto, G.L., Hotza, D., Jahn, S.L., Foletto, E.L., 2019. Preparation of delafossite-type CuFeO₂ powders by conventional and microwave-assisted hydrothermal routes for use as photo-Fenton catalysts. *J. Environ. Chem. Eng.* 7 (2), 102954.
Trusiano, G., Matta, S., Bianchi, M., Rizzi, L.G., Frache, A., 2019. Evaluation of nanocomposites containing graphene nanoplatelets: Mechanical properties and combustion behavior. *Polym. Eng. Sci.* 59 (10), 2062–2071.
Torrizi, V., Ruffino, F., 2015. Metal-polymer nanocomposites: (Co-) evaporation/ (Co) sputtering approaches and electrical properties. *Coatings* 5 (3), 378–424.
Velický, M., Toth, P.S., 2017. From two-dimensional materials to their hetero structures: An electrochemist's perspective. *Appl. Mater. Today* 8, 68–103.
Wahab, R., Ahmad, N., Alam, M., Ahmad, J., 2020a. Formation of composite nanostructures with an effective hydrazine sensor and their chemical approach. *Physica E: Low-Dimens. Syst. Nanostruct.* 117, 113851.
Wahab, R., Khan, F., Yang, Y.B., Hwang, I.H., Shin, H.-S., Ahmad, J., Dwivedi, S., Khan, S.T., Siddiqui, M.A., Saquib, Q., Musarrat, J., Al-Khedhairi, A.A., Mishra, Y.K., Ali, B.A., 2016. Zinc oxide quantum dots: multifunctional candidates for arresting C2C12 cancer cells and their role towards caspase 3 and 7 genes. *RSC Adv.* 6, 26111–26120.
Wahab, R., Khan, F., Al-Khedhairi, A.A., 2018. Hematite iron oxide nanoparticles: apoptosis of myoblast cancer cells and their arithmetical assessment. *RSC Adv.* 8, 24750–24759.
Wahab, R., Siddiqui, M.A., Saquib, Q., Dwivedi, S., Ahmad, J., Musarrat, J., Al-Khedhairi, A.A., Shin, H.-S., 2014. ZnO nanoparticles induced oxidative stress

- and apoptosis in HepG2 and MCF-7 cancer cells and their antibacterial activity. *Colloids Surf. B Biointerfaces* 117, 267–276.
- Wahab, R., Yang, Y.B., Umar, A., Singh, S., Hwang, I.H., Shin, H.S., Kim, Y.S., 2012. Platinum quantum dots and their cytotoxic effect towards myoblast cancer cells (C2C12). *J. Biomed. Nanotechnol.* 8, 424–431.
- Wahab, R., Saquib, Q., Faisal, M., 2020b. Zinc oxide nanostructures: A motivated dynamism against cancer cells. *Process Biochem.* 98, 83–92.
- Wahab, R., Khan, F., A.Siddiqui, M., Ahmad, J., Saquib, Q., Al-Khedhairi, A.A., 2021a. Cytotoxic assessment of liver cancer cells (HepG2) with raw, functionalized multi walled carbon nanotubes and their comparison with nanohydroxyapatite. *J. King Saud Univ. – Sci.* 33 (5), 101444.
- Wahab, R., Siddiqui, M.A., Ahmad, J., Saquib, Q., Al-Khedhairi, A.A., 2021b. Cytotoxic and molecular assessment against breast (MCF-7) cancer cells with cobalt oxide nanoballs. *J. King Saud Univ. Sci.* 33 (5), 101467.
- Wu, F., Wang, C., Hu, H.-Y., Pan, M., Li, H.-F., Xie, N., Zeng, Z., Deng, S., Wu, M.H., Vinodgopal, K., Dai, G.-P., 2019. One-step synthesis of hierarchical metal oxide nanosheet/carbon nanotube composites by chemical vapor deposition. *J. Mater. Sci.* 54 (2), 1291–1303.
- Zhan, F., Wang, R., Yin, J., Han, Z., Zhang, L., Jiao, T., Zhou, J., Zhang, L., Peng, Q., 2019. Facile solvothermal preparation of Fe₃O₄-Ag nanocomposite with excellent catalytic performance. *RSC Adv.* 9 (2), 878–883.